The Astrophysical Journal, 709:369–376, 2010 January 20 doi:10.1088/0004-637X/709/1/369

EXTREME ULTRAVIOLET OBSERVATIONS AND ANALYSIS OF MICRO-ERUPTIONS AND THEIR ASSOCIATED CORONAL WAVES

O. Podladchikova[1], A. Vourlidas[2], R. A. M. Van der Linden[1], J.-P. Wülser[3], and S. Patsourakos[2]
[1] STCE/SIDC, Royal Observatory of Belgium, Ringlaan-3, Brussels 1180, Belgium; Elena.Podladchikova@oma.be, Ronald.Vanderlinden@oma.be
[2] Code 7663, Naval Research Laboratory, 4555 Overlook Ave. SW, Washington, DC 20375, USA; vourlidas@nrl.navy.mil, patsourakos@nrl.navy.mil
[3] Lockheed Martin Solar and Astrophysics Laboratory, Building 252, 3251 Hanover Street, Palo Alto, CA 94304, USA; wuelser@lmsal.com
Received 2009 July 31; accepted 2009 November 25; published 2009 December 31

ABSTRACT

The Solar Terrestrial Relations Observatory EUV telescopes have uncovered small-scale eruptive events, tentatively referred to as "mini-CMEs" because they exhibit morphologies similar to large-scale coronal mass ejections (CMEs). Coronal waves and widespread diffuse dimmings followed by the expansion of the coronal waves are the most brightly manifestations of large-scale CMEs. The high temporal and spatial resolution of the EUV data allows us to detect and analyze these eruptive events, to resolve their fine structure, and to show that the observed "mini-waves" have a strong similarity to the large-scale "EIT' waves. Here, we analyze a micro-event observed on 2007 October 17 by the Sun Earth Connection Coronal and Heliospheric Investigation EUV Imager (EUVI) in 171 Å (Fe IX) with a 2.5 minute cadence. The mini-CME differs from its large-scale counterparts by having smaller geometrical size, a shorter lifetime, and reduced intensity of coronal wave and dimmings. The small-scale coronal wave develops from micro-flaring sites and propagate up to a distance of 40,000 km in a wide angular sector of the quiet Sun over 20 minutes. The area of the small-scale dimming is two orders of magnitude smaller than for large-scale events. The average speed of the small-scale coronal wave studied is 14 km s^{-1}. Our observations give strong indications that small-scale EUV coronal waves associated with the micro-eruptions propagate in the form of slow mode waves almost perpendicular to the background magnetic field.

Key words: Sun: activity – Sun: corona – Sun: coronal mass ejections (CMEs) – Sun: UV radiation – waves

Online-only material: color figures

1. INTRODUCTION

The EUV Imaging Telescope (EIT; Delaboudinière et al. 1995) aboard the *Solar and Heliospheric Observatory* (*SOHO*) mission made significant progress possible in the understanding of the low coronal manifestations of coronal mass ejections (CMEs). The large-scale perturbations of the coronal magnetic field during the onset of CMEs manifest themselves most spectacularly by EUV dimmings and coronal "EIT" waves (Aschwanden 2004; Nakariakov & Verwichte 2005). Dimmings are transient coronal holes appearing during the onset of CMEs around the source regions (Hudson & Webb 1997; Webb 2000). They are best observed as large areas of intensity decrease in soft X-Ray and EUV radiation (Bewsher et al. 2008). Propagating bright fronts ("EIT" waves) are often seen ahead of the outer dimming borders.

Bright fronts of coronal waves propagate from eruption centers with velocities of a few hundred km s^{-1} (Thompson et al. 1998; Long et al. 2008; Patsourakos et al. 2009). They are followed by an expanding dimming region (Klassen et al. 2000; Warmuth et al. 2001; Podladchikova & Berghmans 2005a). When the magnetic structure on the solar surface is simple, EIT waves have a quasi-isotropic character and propagate in wide angular sectors more or less symmetrically with respect to the eruption center (Moses et al. 1997; Klassen et al. 2000; Warmuth et al. 2001; Podladchikova & Berghmans 2005a).

The properties of coronal waves are strongly affected by their interaction with active regions and coronal holes. Waves have been observed to stop at or avoid active regions and to reflect at coronal hole boundaries (Ofman & Thompson 2002; Gopalswamy et al. 2009; Chen et al. 2005a; Delannée 2000; Podladchikova & Berghmans 2005c).

Full sun synoptic images from the EUVI telescope (Wuelser et al. 2004) of the Sun Earth Connection Coronal and Heliospheric Investigation (SECCHI) imaging suite (Howard et al. 2008) in 171 Å with a cadence of 2.5 minutes and pixel size of 1.59 arcseconds have revealed events with an apparent morphology similar to coronal waves and CMEs, but with considerably smaller sizes. The events occur on the quiet Sun and at the peripheries of active regions and are often accompanied by small filament eruptions, EUV dimmings, and propagating wave-like disturbances. The coronal eruptions of similar scales have been studied in few cases only. High-resolution ground-based observations have revealed a number of small-scale filaments observed in the quiet Sun areas. Small-scale filament eruptions appear to be the counterparts of large-scale ones (Hermans & Martin 1986; Sakajiri et al. 2004; Wang et al. 2000; Ren et al. 2008). Ren et al. (2008) reported about the multi-wavelength observation of an eruptive tiny filament resulting in coronal micro-dimmings as observed by 195 Å EIT channel. This small-scale filament shows the similar characteristics as the previous findings in the large-scale filament eruptions associated with CMEs. Some statistics of small-scale SECCHI eruption properties and their association with the underlying photospheric magnetic field have been presented recently by Innes et al. (2009). They showed that some of the eruptions may be the result of converging supergranular flows and suggested that the small-scale dimmings may be the result of propagating mini-EIT waves. Robbrecht et al. (2009) demonstrated that small-scale CMEs exist in the outer corona. Small-scale coronal jets are also observed in EUV and X-ray solar corona (Koutchmy et al. 1998; Filippov et al. 2007; Filippov et al. 2009).

In this paper, we focus on the small-scale diffuse coronal fronts and their associated widespread dimmings seen by

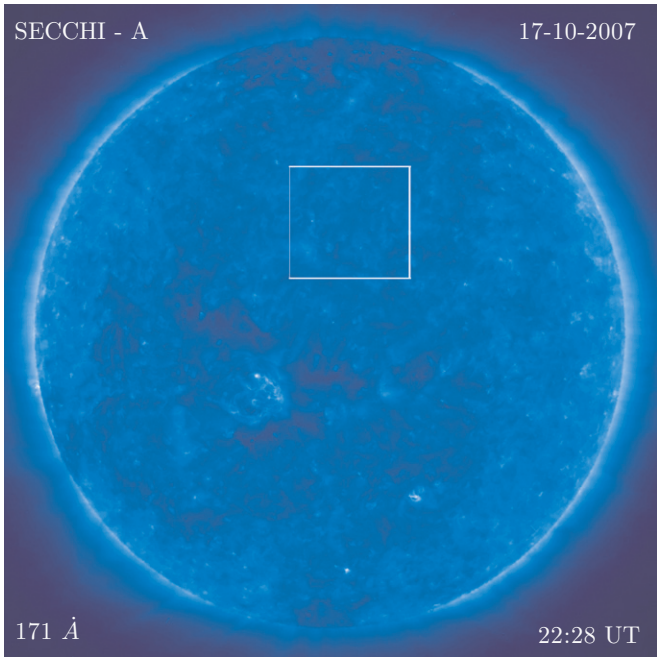

Figure 1. SECCHI/STEREO 171 Å direct image at 22.28 UT on 2007 October 17. The square delineates the quiet-Sun area of 261 × 261 pixels where three small-scale events similar to CMEs were found.

(A color version of this figure is available in the online journal.)

SECCHI/EUV imager. We explore in detail the nature of these propagating disturbances to see whether they could be waves. The small-scale coronal wave and dimming structures are not easy to resolve, and a multitude of other small-scale activity interferes with the measurements of the physical parameters of these events using standard techniques. Therefore, we employ the technique of coronal wave and dimming extraction described in detail by Podladchikova & Berghmans (2005a). We demonstrate the full analogy of coronal waves structure and evolution of *SOHO*/EIT macro-events and SECCHI/EUVI micro-events.

2. EUVI OBSERVATIONS OF MINI-WAVES ON 2007 OCTOBER 17

The micro-eruptions of 2007 October 17 occurred on the quiet-Sun under a simple solar magnetic field configuration and in the absence of large active regions on the Sun. To study these events, we used the EUVI images from the Solar Terrestrial Relations Observatory (STEREO) ahead spacecraft (EUVI-A). Figure 1 shows the SECCHI/STEREO 171 Å image at 22.28 UT. The events under study occurred within a 261 × 261 pixels (415 × 415 arcseconds) square in the northern hemisphere of the Sun. Three micro-events were observed in this region marked by the white square between 22:13 UT and 22:38 UT. The direct image of this subfield is shown in Figure 2(a) at 22:11 UT.

To analyze the geometrical structure and properties of these events, we formed fixed difference (FD) images. Such images are formed by the subtraction of a prevent image (22:11 UT) from the next ones, taking into account the differential rotation of the Sun. FD images are shown in Figures 2(b)–(h) at 22:16 UT, 22:18 UT, 22:21 UT, 22:23 UT, 22:26 UT, 22:28 UT, 22:31 UT, and 22:33 UT, respectively. The small-scale eruptions occur almost simultaneously in that region and are marked by the three squares. Bright fronts and dimmings propagate from the eruption center toward a northeast direction (top left square).

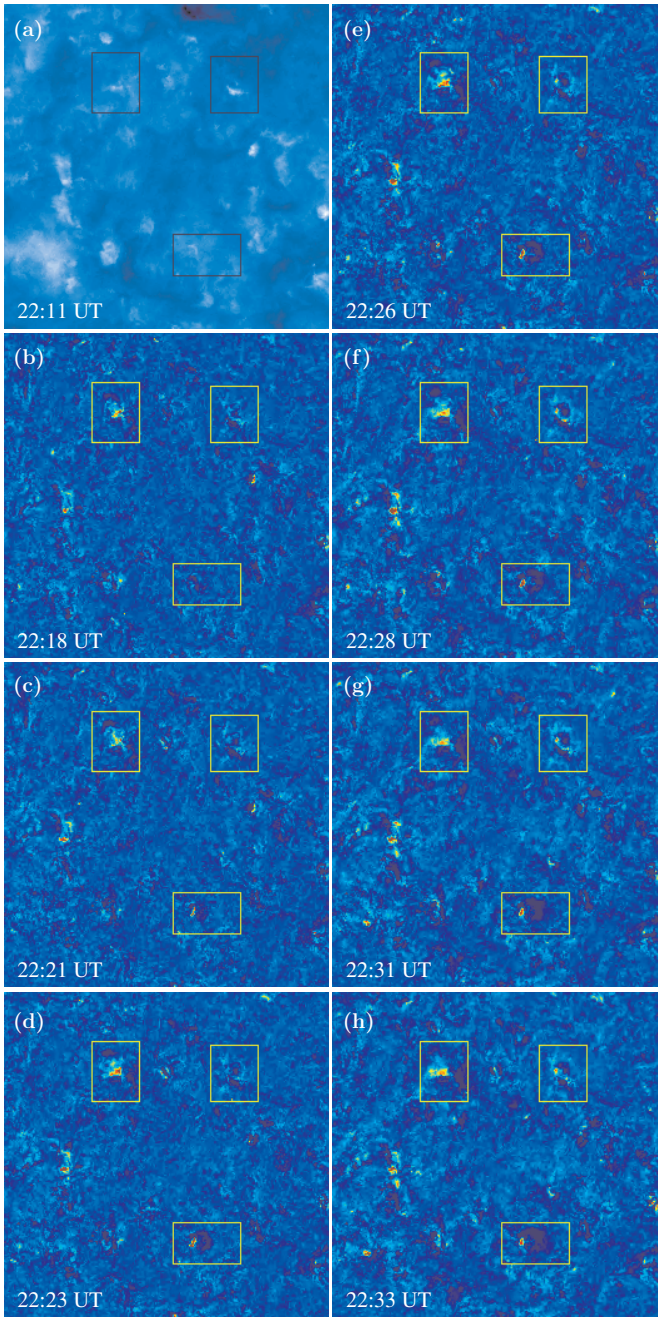

Figure 2. Extracted fields of the SECCHI/STEREO 171 Å image on Figure 1. The first frame (a) is a direct image, while the others are fixed difference images, which are obtained by subtracting the pre-event image at 22:11 UT. Three small-scale EUV coronal waves develop simultaneously during the time interval 22:16 UT–22:33 UT. The dynamic evolution of waves is illustrated by undifferenced and differenced animations at http://sidc.be/nemo/micro. In this paper, we analyze in detail the bottom EUV wave enclosed by the [30 × 50] pixels or [50 × 80] arcseconds square.

(A color version of this figure is available in the online journal.)

The development of micro-structures takes place mainly toward a northwest direction (top right square). A rather symmetrical expansion of the dimming and coronal wave is observed in a wide angular sector in the western direction (bottom square). Animation 1 shows these data dynamically and can be found at http://sidc.be/nemo/micro. Animation 2 shows the original images dynamically.

The simultaneous occurrence of those micro-events could be considered as an argument for the magnetic connection between them or it could be a random occurrence. More detailed studies

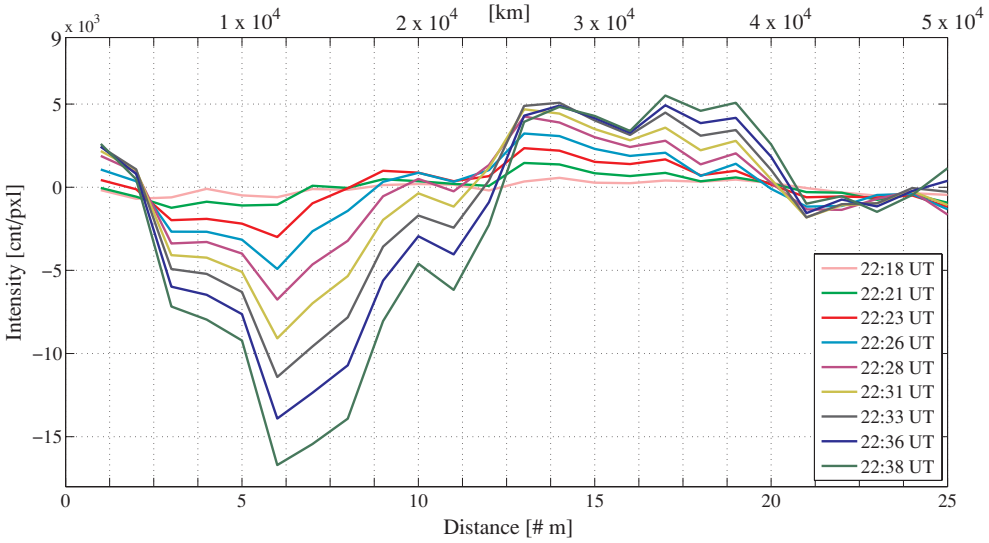

Figure 3. Ring analysis applied on the bottom micro-event in Figure 2. It shows the total intensity per ring over the 25 consecutive rings, m, constructed around the onset site for different times. Each curve shows three distinct regions: Eruption area—positive intensities near onset site ($0 < m \leqslant 2$); dimming region—negative intensities ($m > 2$); wave front—positive intensities at the outer border of dimming.

are required before reaching a firm conclusion on that point. Here we focus on the bottom event. We investigate its dimming structure and associated wave dynamics.

3. SMALL-SCALE CORONAL WAVE VELOCITY DEFINITION USING RING ANALYSIS

The algorithm of ring analysis (Podladchikova & Berghmans 2005a; Attrill et al. 2007; Podladchikova & Berghmans 2005b) is used for the precise location of the dimming and the wave front relative to the eruption center. We introduce a polar coordinate system $[r, \varphi]$ on the solar sphere with the coordinate center's origin in the eruption center's brightest point at time 22:28 UT. (At this time the intensity at the eruption center reaches its maximum value.) The angle φ is measured counter-clockwise starting from the vertical downward, i.e., all points on the sphere vertically below the eruption center correspond to $\varphi = 0$. The angle φ increases from 0 to 2π. Below we present the detailed analysis of intensity variations for the 2007 October 17 micro-event in such a polar coordinate system.

The dimming development is most impressive toward the west direction. Therefore, the west side between the event center and active areas is covered by 20–25 semi-rings (approximately 40,000–50,000 km). For every semi-ring m, we estimate the total intensity $S(m)$ as the sum of all pixel intensities belonging to this semi-ring ($m = 1, 2, \ldots, 25$). Figure 3 shows the dependence of the integral intensities of the semi-rings on number m (or distance r_m from the eruption center) for the FD images in Figure 2. Plots for all nine curves have similar forms. From these plots, we can define the locations of the small-scale eruption center region, the dimming region and the coronal wave using the zeros of S_m. The intensity is largest for the semi-rings between $m = 1$ and $m = 2.3$, close to the eruption center. The region of intensity decrease ($m_1 < m < m_2$) corresponds to the dimming ($m_1 = 2.3$, $m_2 = 7$ at 22:21 UT; $m_1 = 2.3$, $m_2 = 13$ at 22:38 UT). The curve for 22:18 UT shows that the dimming appears *before* the micro-flare brightening. The dimmings monotonously expand and become darker during this time interval.

The internal border of the coronal wave front moves away from the micro-flaring site (from $m = 7$ at 22:21 UT to $m = 13$ at 22:38 UT). However, the external border of the coronal wave front ($m = 21$ at 22:33 UT) appears to stop at 22:38 UT. It is also possible that small-scale coronal wave stop and/or are reflected by other magnetic structures, in a way similar to large-scale coronal EUV waves (Gopalswamy et al. 2009; Chen et al. 2005b; Delannée 2000). This effect could be caused by interaction with other weak active regions that are observed as areas of high and low intensity (see Figure 2) located 40,000–50,500 km ($m = 20$–25) to the west, the northwest, and the southwest of the event center. Therefore, we estimate the speed of the internal wave front border which was not deformed by the interaction with other active regions and is defined only by its origin and mechanism of generation. Between 22:21 UT and 22:38 UT, the internal border of the wave front moved from $m = 7$ to $m = 13$. The average front speed is therefore $V = 14$ km s^{-1}, defined as the difference of the distances divided by the time interval.

3.1. Small-scale Coronal Wave and MHD Waves

Our analysis shows that the small-scale coronal wave travels a distance of 40,000 km from the eruption center with an average front speed $V = 14$ km s^{-1}. This velocity is substantially smaller than the velocity of a sound wave moving strictly along the magnetic field lines. The value of $C_{\rm sound}$ for the considered layers of the EUV solar corona is approximately equal to 200 km s^{-1} (Démoulin & Klein 2000). However, in the limit $V_A \gg V_S$ for the coronal layers we study, the velocity of slow magneto-acoustic mode strongly depends upon the angle to the background magnetic field as

$$V_{\rm slow} = C_{\rm sound} \cdot \cos\theta, \quad (1)$$

(see Figure 4(a) for the graphical representation of this dependence). From Equation (1), we conclude that the small-scale EUV coronal event we study in detail here corresponds to a slow magneto-acoustic mode propagating at an angle of 86° to the background magnetic field directed perpendicular to solar surface, similar to some large-scale events (Wu et al. 2005; Krasnoselskikh & Podladchikova 2007; Gilbert et al. 2008; Wang et al. 2009).

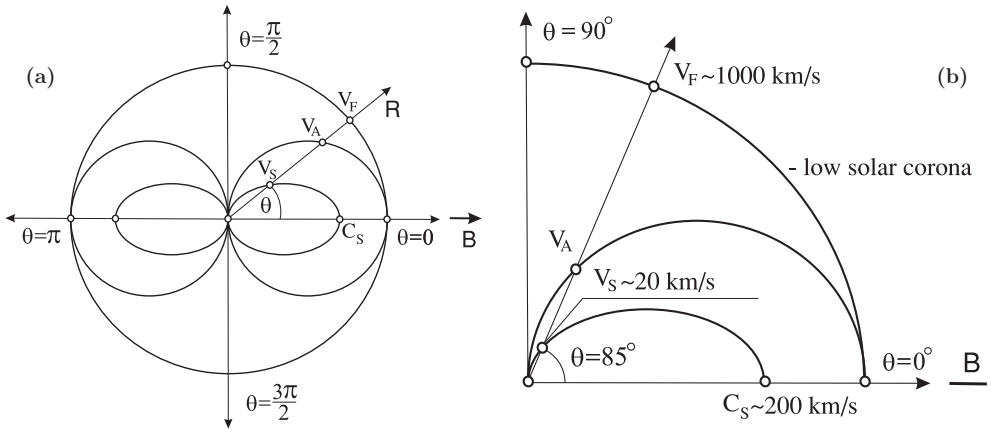

Figure 4. Phase velocities of linear magnetohydrodynamic waves for (a) general case and (b) specific EUV solar corona parameters. Slow and Alfvén wave speeds V_S and V_A vary with θ, the angle between wave propagation and the background magnetic field **B**. The SECCHI mini-wave observed on 2007 October 17 corresponds to a slow magneto-acoustic wave propagating with velocity V_S at an angle of 86° to **B**.

Such observed speeds exclude other MHD modes from consideration. The angular dependence of the fast magneto-acoustic mode on the angle θ is very weak (see Figure 4(b)), and as a consequence the fast mode has a rather circular character of propagation. Its speed V_F is very large, of the order of the Alfvén speed, which is around 1000 km s^{-1} here (Démoulin & Klein 2000). Thus, the small-scale EUV coronal wave associated with the micro-eruption we observe here cannot be a fast magneto-acoustic wave. At the same time, the Alfvén wave speed V_A also changes with θ. Thus, the oblique Alfvén wave can also have a very small velocity. However, the Alfvén wave is essentially a magnetic field perturbation and cannot create such a large amplitude density/intensity perturbation.

3.2. Other Mechanisms of Coronal Wave Formation

Large-scale coronal "EIT" waves observed by *SOHO* differ from the majority of chromospheric waves (Moreton 1960) first by the essentially smaller speeds (thousand versus hundreds km s^{-1}). Second different aspect is the deviation of "EIT" wave front form the circular shape. The second different aspect is the deviation of "EIT" wave front form the circular shape. The behavior of fast chromospheric waves corresponds rather to the fast magneto-acoustic mode (Uchida 1974). The unique fast EUV wave caught by the *Transition Region and Coronal Explorer* also shows the properties of the fast magneto-acoustic mode (Wills-Davey & Thompson 1999; Ofman & Thompson 2002; Ballai et al. 2005).

Wang (2000) and Wu et al. (2005) have shown numerically that the perturbation initiated by a flare or filament explosion should propagate because of the fast magneto-acoustic wave and the slow magneto-acoustic mode in different layers of solar corona. Warmuth et al. (2001) have demonstrated the co-spatiality at least of some simultaneously propagating global waves of different speeds in the chromosphere and in the corona. Using spectral diagnostics, Harra & Sterling (2003) have demonstrated for a particular event that a coronal wave consists of two aspects: a slow wave followed by a strong dimming region and a faint wave moving essentially faster. Gilbert et al. (2008) gave the evidence that even a slowly propagating chromospheric wave displays the properties of the slow magneto-acoustic mode. Krasnoselskikh & Podladchikova (2007) have presented more signatures of slow "EIT" waves that correspond to the slow MHD mode.

Nevertheless, there is a possibility of "EIT" wave formation by alternative mechanisms. Delannée (2000) proposed an idea of front formation by plasma compression on the expanding dimming border. Attrill et al. (2007) have introduced the idea of "EIT" wave front formation by magnetic energy dissipation, namely by the multiple driven reconnections between the magnetic flux of a dimming and small-scale magnetic loops in the background magnetic field. Delannée et al. (2008) have elaborated an extended model of front formation by current shells.

Chen et al. (2005a) have demonstrated that different mechanisms proposed for global coronal wave formation can be united in one scheme, as for example plasma compression and compression wave represent the same phenomenon described in different terms. Plasma compression in its turn can serve as the driver for the reconnection processes (Parker 1957). Zhukov & Auchère (2004) have described "EIT" waves as bimodal phenomenon showing both the wave properties and the opened magnetic flux signatures. Therefore, the possibility of small-scale SECCHI phenomenon to be created by non-MHD-wave mechanisms should be studied in quantitative terms in the future.

4. ANGULAR STRUCTURE OF MICRO-DIMMINGS

We now turn to a comparison of the angular structure, intensity, and area of the observed small-scale dimmings to the properties of the large-scale dimmings observed in association with CMEs.

4.1. The Sector Analysis of Dimmings

To study the direction of dimming propagation, we divide the semi-ring $0 < \varphi \leqslant \pi$ into four equal sectors. The integral intensity $S(m, k)$ is defined as the total intensity of all pixels that belong to semi-ring m and sector k, such that $\sum_{k=1}^{4} S(m, k) = S(m)$. Figure 5 shows the dependence of the integral intensities $S(m, k)$ on the semi-ring number m for FD images at 22:23 UT (Figure 5(a)) and 22:31 UT (Figure 5(b)) in all four sectors. As shown in Figure 5(a), the dimming develops rather simultaneously in all four sectors, though the intensity of dimming varies in each sector. By the end of the event development at 22:31 UT (Figure 5(b)), the dimming appears essentially anisotropic. The local drop of the intensity in the sector $3\pi/4 < \varphi \leqslant \pi$ (blue curve) at the distance 6000–9000 km (m = 3–4) from the eruption center shows a small deep

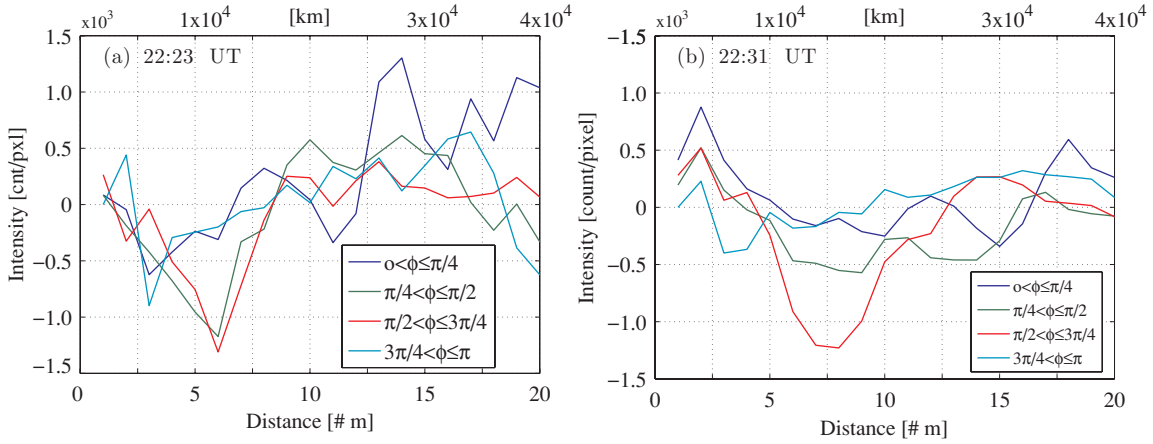

Figure 5. Sector analysis showing the angular structure of the micro-eruption. The dependence of integral intensity $S(m, k)$ on the ring number m is shown for each angular sector $k = 1, 2, 3, 4$. (a) Illustration of relatively synchronous dimming development in the early stage of the event (at 22:23 UT). (b) Dimming becomes anisotropic at the later stages (22:31 UT). The localized ($m = 3$–4) drop in the intensity (blue curve) shows a small deep dimming close to the eruption center that expands with a lower velocity than other areas.

dimming that expands with the essentially lower velocity than a dimming in other sectors.

The external border of the dimming in the angular sector $\pi/4 < \varphi \leqslant \pi/2$ (green curve) extends to 35,700 km ($m = 17$), while in other angular sectors the dimming extends only to distance 18,000–27,400 km ($m = 9$–13). The dimming has the form of an extended narrow structure. A similar shape for large-scale dimmings is observed when the magnetic structure of the surrounding atmosphere is sufficiently complex (Chen et al. 2005b; Podladchikova & Berghmans 2005c). The evolution of the large-scale dimmings can be strongly affected by magnetic structures of similar scales. They are observed in the area of propagation of the investigated event.

Thus, the dynamics of micro-dimmings shows the following properties:

1. The dimming develops synchronously and quasi-isotropically in a wide angular sector around the micro-flaring site in the quiet area of the Sun.
2. The dimming becomes anisotropic during the late stage of development similar to the behavior of large-scale dimmings (Podladchikova & Berghmans 2005a; Chen et al. 2005a; Attrill et al. 2007).

4.2. Total Intensity and Micro-dimming Area Dynamics

To study the dynamics of the small-scale dimming propagation, we extract the dimmings and estimate the area and integral intensity of this region for a 13 minutes interval (22:18 UT–22:31 UT). The small-scale dimming extraction was identical to the growing region technique used in large-scale dimming extraction (Podladchikova & Berghmans 2005a); see, e.g., techniques by de Wit (2006), Nakariakov & King (2007), Attrill et al. (2006), and Robbrecht & Berghmans (2005) for the review of growing regions techniques.

First, from the fixed differences of images corrected for differential rotation, we extracted small regions with dimmings. Then, from these images we extracted two regions: a region corresponding to the lowest intensities, where each pixel certainly belongs to the dimming, and a region of weaker, but still lower intensity in comparison to the image before the event occurrence. This second region also includes weak dimmings around intensive ones, artifacts, and other phenomena not connected with dimmings. To filter out phenomena not connected to the dimmings propagation, we build up the final dimming from the most intensive dimmings, adding pixels of less intensive dimming only if they are connected to the strong dimming region. A similar procedure is applied to extract the onset site brightenings.

Figure 6 shows three different views of the 2007 October 17 SECCHI/EUVI-A micro-eruption. Top panel (Figure 6(a)) shows a direct image of the small-scale magnetic loop at the onset site, which becomes brighter at 22:18 UT. Figure 6(b) shows the final dimmings and the micro-flaring site after the operation of its extraction from FD 22:18 UT, 22:21 UT, 22:23 UT, 22:26 UT, 22:28 UT, and 22:31 UT. The micro-dimming was formed before a brightening at the onset site and expands intensively starting at 22:21 UT at the time of the flare brightening. It suggests that at least part of the micro-dimming is due to absorption by an erupting filament.

We extract the deep core dimming connected with the activity of the magnetic loop footpoint. This deepest dimming region with the pixels of the strongest negative intensity is presented in Figure 6(c). The deep dimming was formed before a brightening at the onset site and remained the deepest throughout all observation time. It is located north to the onset site, while the full micro-dimming expands in a wide angular sector around the micro-flaring site. This part of the extracted dimming does not show wave-like signatures. The same conclusion follows from the consideration of the micro-dimming intensities in the different angular directions (blue curve in Figure 5).

The area and the integral intensity of the full micro-dimming evolve monotonously in time as shown in Figures 7(a) and 7(b), while the intensity of the deep dimming core starts to decrease sharply at 22:21 UT and reaches its maximum at 22:23 UT (Figure 7(c)). An intensity increase in the onset site correlates with an abrupt intensity decrease in the deep dimming, which starts to decrease 2 minutes prior to the onset site brightening (Figure 7(d)). The duration of the full micro-dimming development exceeds considerably the time of the micro-flare explosive phase, which is another similarity to the large-scale dimming evolution during CMEs (Webb et al. 2000).

In Table 1, we show a comparison of the maximum values of dimming areas of the micro-dimmings observed by SECCHI/EUVI and large-scale dimmings accompanying the 1997 May 12 CME (see analysis of EIT/*SOHO* data by Podladchikova & Berghmans 2005a). The dimming area of the EUV wave on

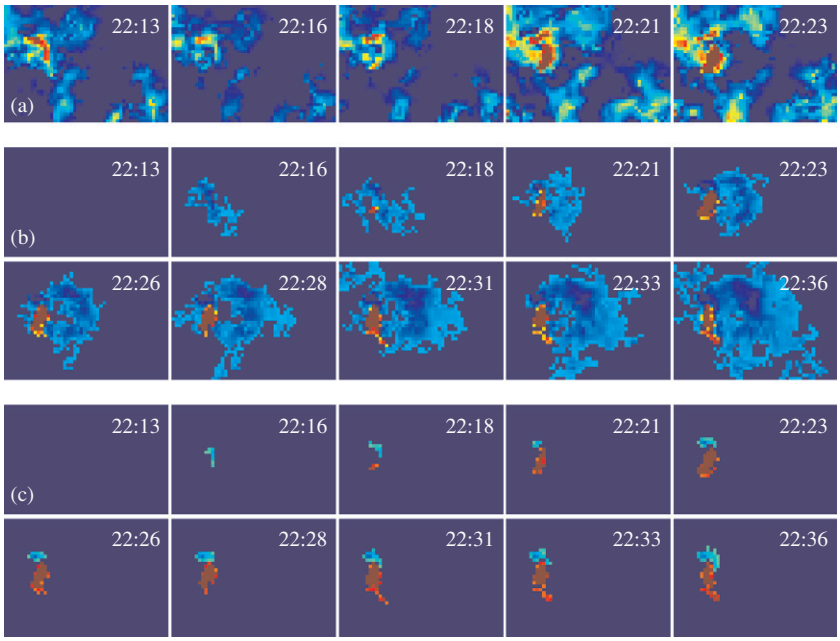

Figure 6. Three different views of the 2007 October 17 SECCHI/EUVI-A micro-eruption: (a) Direct image—small-scale magnetic loop at the onset site becomes brighter at 22:18 UT; (b) A brightening at the onset site (red) and the micro-dimming (blue), extracted from the differenced images. Micro-dimming expands in a wide angular sector around the micro-flaring site starting at 22:21 UT. (c) The deepest micro-dimming part, which contains pixels of the strongest negative intensity. It adjoins directly the flaring site (see blue curve in Figure 5). The micro-dimming appears at 22:16 UT whereas the micro-flare brightening appears only at 22:18 UT. The box is [30 × 50] pixels or [50 × 80] arcsecs in size. See Figure 7 and Table 1 for parameters.

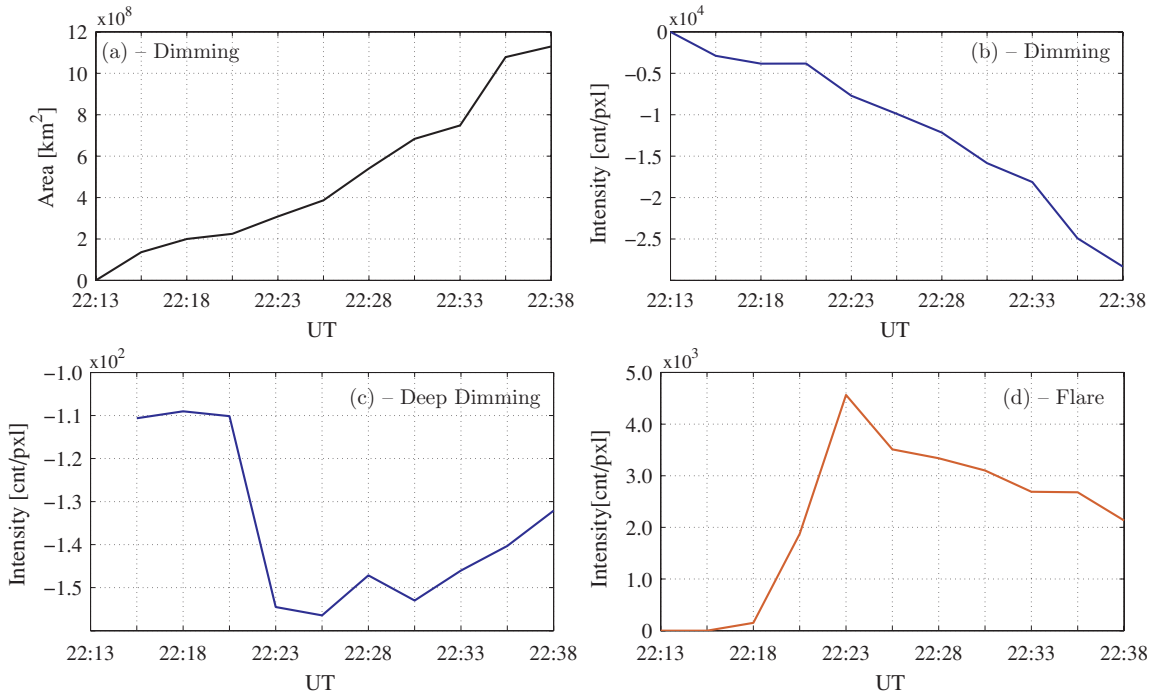

Figure 7. (a) Micro-dimming area evolution. (b) The micro-dimming integral intensity evolution. (c) Evolution of the micro-dimming minimal intensity (deep dimming on the Figure 6). (d) The micro-flare integral intensity evolution. Micro-dimming is developing monotonously throughout the event observation, frames (a) and (b). Dimming minimal intensity drops abruptly in correlation with the micro-flaring explosive phase, frames (c) and (d).

1997 May 12 was more than two orders of magnitude larger than the measured characteristics of the micro-dimming observed on 2007 October 17 by SECCHI.

5. DISCUSSION AND CONCLUSIONS

The SECCHI/EUVI observations reveal the existence of numerous small-scale eruptions accompanied by dimmings and coronal waves. These characteristics are very similar to low corona eruptions associated with large-scale CMEs. Our detailed analysis of EUVI differentially derotated fixed differences images taken on 2007 October 17 in the 171 Å (Fe IX) wavelength allow us to extract the properties of small-scale dimmings and waves and compare them with their large-scale counterparts. Our findings can be summarized as follows.

1. The bright front of a small-scale coronal wave is observed ahead of the dimming's external edge, similar to large-scale

Table 1
Integrated Characteristics of Micro-eruption Resolved by SECCHI/STEREO versus Large-scale Eruption (EIT/*SOHO*)

PARAMETER	SECCHI/STEREO Micro-eruption 17/10/07	EIT/*SOHO* Macro-eruption 12/05/97
Dimming area $[km^2]$	$1.0 \times 10^8 \div 1.0 \times 10^9$	2.0×10^{11}
Average front speed	14 km s^{-1}	247 km s^{-1}

events. However, it propagates up to 40,000 km from the eruption center with a speed approximately 10–20 times smaller (14 km s^{-1}) than a large-scale coronal wave.

2. This speed is an order of magnitude smaller than the sound speed in these layers of the solar corona (and two orders of magnitude smaller than the fast magneto-acoustic or Alfvén wave speeds). However, the speed of the slow magneto-acoustic wave depends strongly on the angle of propagation. Our SECCHI wave event corresponds to a slow magneto-acoustic wave propagating at an angle of 86° to the background magnetic field. Different non-wave mechanisms recently proposed for coronal wave formation should also be considered and quantified in application to small-scale SECCHI events. Among them are the magnetic mechanisms (current layers formation at the outer border of dimmings) and plasma compression by the expanding dimming structures. Let us note that plasma compression processes represent just different description of wave phenomena.
3. Similar to the large-scale CME, a coronal dimming appears to be of two types: deep core dimmings, sometimes shown to correspond to the footpoints of the erupted flux rope (Webb et al. 2000), and a more widespread dimming, observed to correspond well to the spatial extent of CMEs. The formation of small-scale dimmings starts a few minutes before the associated small-scale flare brightening. The explosive phase of micro-flare lasts 5 minutes. However, the duration of the dimming evolution covers a longer time (>20 minutes) and continues even after the decrease in the micro-flare intensity similar to large-scale events dynamics.
4. The micro-dimming and wave show initially a quasi-isotropic development and waves in the quiet area of the solar surface. The small-scale coronal wave stops at active regions (even very weak ones) similar to large-scale events. The late dimming development acquires a strongly anisotropic character. The micro-dimmings area is two orders of magnitude smaller than those of a large-scale dimmings.

In summary, we carried out a detailed study of a small-scale eruption event. The structure as a whole and the details of its development show strong morphological similarities with coronal eruptions that accompany large-scale CMEs. The micro-eruptions have substantially smaller scales in all of their properties (intensity, geometrical sizes, lifetime, and speed). The study of such details of EUV eruptions observed in the corona is possible due to the essentially improved spatial and temporal resolution of EUVI instrument with respect to EIT. The straightforward adoption of techniques for the extraction of dimming and wave properties from large-scale events demonstrates the close similarity between the two classes. They could, therefore, be considered as EUV micro-waves and micro-dimmings.

We thank an anonymous referee for many constructive suggestions that substantially improved the paper. The SECCHI data used here were produced by an international consortium of the Naval Research Laboratory (USA), Lockheed Martin Solar and Astrophysics Lab (USA), NASA Goddard Space Flight Center (USA), Rutherford Appleton Laboratory (UK), University of Birmingham (UK), Max-Planck-Institut for Solar System Research (Germany), Centre Spatiale de Liège (Belgium), Institut d'Optique Théorique et Appliqueé (France), and Institut d'Astrophysique Spatiale (France). O.P. thanks V. Krasnoselskikh, E. Robbrecht, and M. Velli for fruitful discussions.

REFERENCES

Aschwanden, M. 2004, Physics of the Solar Corona: An Introduction (Springer-Praxis Books in Geophysical Sciences; Berlin: Springer)
Attrill, G. D. R., Harra, L. K., van Driel-Gesztelyi, L., & Démoulin, P. 2007, ApJ, 656, 101
Attrill, G., Nakwacki, M. S., Harra, L. K., van Driel-Gesztelyi, L., Mandrini, C. H., Dasso, S., & Wang, J. 2006, Sol. Phys., 238, 117
Ballai, I., Erdélyi, R., & Pintér, B. 2005, ApJ, 633, 145
Bewsher, D., Harrison, R. A., & Brown, D. S. 2008, A&A, 478, 897
Chen, P. F., Ding, M. D., & Fang, C. 2005a, ApJ, 622, 1202
Chen, P. F., Fang, C., & Shibata, K. 2005b, Space Sci. Rev., 121, 201
de Wit, T. D. 2006, Sol. Phys., 239, 519
Delaboudinière, J. P., et al. 1995, Sol. Phys., 162, 291
Delannée, C. 2000, ApJ, 545, 512
Delannée, C., Török, T., Aulanier, G., & Hochedez, J. F. 2008, Sol. Phys., 247, 123
Démoulin, P., & Klein, K. 2000, in Transport and Energy Conversion in the Heliosphere, Structuring of the Solar Plasma by the Magnetic Field, ed. J. P. Rozelot, L. Klein, & J. C. Vial (Lecture Notes in Physics, Vol. 553; Berlin: Springer), 99
Filippov, B., Golub, L., & Koutchmy, S. 2009, Sol. Phys., 254, 259
Filippov, B., Koutchmy, S., & Vilinga, J. 2007, A&A, 464, 1119
Gilbert, H. R., Daou, A. G., Young, D., Tripathi, D., & Alexander, D. 2008, ApJ, 685, 629
Gopalswamy, N., et al. 2009, ApJ, 691, 123
Harra, L. K., & Sterling, A. C. 2003, ApJ, 587, 429
Hermans, L. M., & Martin, S. F. 1986, in NASA Conference Publication 2442, Goddard Space Flight Center Coronal and Prominence Plasmas, ed. A. I. Poland (Washington, DC: NASA Publication Division), 369
Howard, R. A., et al. 2008, Space Sci. Rev., 136, 67
Hudson, H. S., & Webb, D. F. 1997, in Coronal Mass Ejection, Yohkoh SXT Observations of X-ray "Dimming" Associated with a Halo Coronal Mass Ejection, ed. J. Crooker, J. A. Joselyn, & J. Feynman (AGU Geophysical Monograph Series 99; Washington, DC: American Geophysical Union), 27
Innes, D. E., Genetelli, A., Attie, R., & Potts, H. E. 2009, A&A, 495, 319
Klassen, A., Aurass, H., Mann, G., & Thompson, B. J. 2000, A&AS, 141, 357
Koutchmy, S., Hara, H., Shibata, K., Suematsu, Y., & Reardon, K. 1998, in Observational Plasma Astrophysics: Five Years of YOHKOH and Beyond, SXR Coronal Polar Jets and Recurrent Flashes, ed. T. Watanabe, T. Kosugi, & A. C. Sterling (Astrophysics and Space Science Library, Vol. 229; Boston, MA: Kluwer), 87
Krasnoselskikh, V., & Podladchikova, O. 2007, Are EIT waves slow mode blast waves? (AGU Fall Meeting Abstracts; Washington, DC: American Geophysical Union), 1047
Long, D. M., Gallagher, P. T., McAteer, R. T. J., & Bloomfield, D. S. 2008, ApJ, 680, 81
Moreton, G. E. 1960, AJ, 65, 494
Moses, D., et al. 1997, Sol. Phys., 175, 571
Nakariakov, V. M., & King, D. B. 2007, Sol. Phys., 241, 397
Nakariakov, V. M., & Verwichte, E. 2005, Living Rev. Sol. Phys., 2, 3
Ofman, L., & Thompson, B. J. 2002, ApJ, 574, 440
Parker, E. N. 1957, J. Geophys. Res., 62, 509
Patsourakos, S., Vourlidas, A., Wang, Y. M., Stenborg, G., & Thernisien, A. 2009, Sol. Phys., 259, 49
Podladchikova, O., & Berghmans, D. 2005a, Sol. Phys., 228, 265
Podladchikova, O., & Berghmans, D. 2005b, Energetic Dymanics of EIT Wave Structure Analyzed by EIT Wave Detector, Solar Wind 11/SOHO 16, Connecting Sun and Heliosphere, ed. B. Fleck, T. H. Zurbuchen, & H. Lacoste (ESA SP-592; Noordwijk: ESA Publications Division), 751

Podladchikova, O., & Berghmans, D. 2005c, in Solar Wind 11/SOHO 16, Connecting Sun and Heliosphere, ed. B. Fleck, T. H. Zurbuchen, & H. Lacoste (ESA SP-592; Noordwijk: ESA Publications Division), 535
Ren, D. B., Jiang, Y. C., Yang, J. Y., Zheng, R. S., Bi, Y., & Wang, M. 2008, Ap&SS, 318, 141
Robbrecht, E., & Berghmans, D. 2005, Sol. Phys., 228, 239
Robbrecht, E., Berghmans, D., & Van der Linden, R. A. M. 2009, ApJ, 691, 1222
Sakajiri, T., et al. 2004, ApJ, 616, 578
Thompson, B. J., Plunkett, S. P., Gurman, J. B., Newmark, J. S., St.-Cyr, O. C., & Michels, D. J. 1998, Geophys. Res. Lett., 25, 2465
Uchida, Y. 1974, Sol. Phys., 39, 431
Wang, H., Shen, C., & Lin, J. 2009, ApJ, 700, 1716
Wang, Y. M. 2000, ApJ, 543, 89
Wang, J., Li, W., Denker, C., Lee, C., Wang, H., Goode, P. R., McAllister, A., & Martin, S. F. 2000, ApJ, 530, 1071
Warmuth, A., Vršnak, B., Aurass, H., & Hanslmeier, A. 2001, ApJ, 560, 105
Webb, D. F. 2000, J. Atmos. Sol.-Terr. Phys., 62, 1415
Webb, D. F., et al. 2000, J. Geophys. Res., 105, 27251
Wills-Davey, M. J., & Thompson, B. J. 1999, Sol. Phys., 190, 467
Wu, S. T., Li, B., Wang, S., & Zheng, H. 2005, J. Geophys. Res., 110, 11102
Wuelser, J. P., et al. 2004, Proc. SPIE, 5171, 111
Zhukov, A. N., & Auchère, F. 2004, A&A, 427, 705